Institute of Paper Science and Technology
Atlanta, Georgia

IPST TECHNICAL PAPER SERIES

NUMBER 494

COMPUTATIONAL ANALYSIS OF TWO-PHASE SHEAR FLOWS

J.F. MC KIBBEN AND C.K. AIDUN

JULY 1993

Computational Analysis of Two-phase Shear Flows

J.F. McKibben and C.K. Aidun

Submitted to
1993 TAPPI Engineering Conference
September 20–23, 1993
Orlando, Florida

COMPUTATIONAL ANALYSIS OF TWO-PHASE SHEAR FLOWS

John F. McKibben
Doctoral Candidate
Institute of Paper Science and Technology
Atlanta, GA 30318
USA

Cyrus K. Aidun
Associate Professor
Institute of Paper Science and Technology
Atlanta, GA 30318
USA

ABSTRACT

The size distribution of black liquor droplets sprayed into a Kraft recovery furnace can have a dramatic effect on furnace efficiency and safety. We have developed a computational fluid dynamics tool which will allow study of the processes leading to the breakup of a sheet of black liquor into individual droplets. This is accomplished by solving the full Navier-Stokes equations describing the flow within the black liquor coupled with a potential flow solution in the vapor phase. Results are presented showing the accuracy of our technique in predicting the stability of a planar viscous liquid sheet flowing through a stagnant, inviscid vapor phase.

INTRODUCTION

The process of spraying black liquor into a recovery furnace is important to the operation and efficiency of the furnace, with particular emphasis placed on the distribution of the black liquor droplet sizes. If droplets are too small, they will tend to be entrained in the upward flowing flue gas leading to fouling of the heat transfer surfaces. Droplets which are too large may not dry completely prior to reaching the char bed, leading to low bed temperatures and inefficient sulfur reduction.

One typical method used for black liquor spraying is a splash-plate show in Figure 1. This process involves a jet of black liquor impinging on a flat plate, the liquor is then deflected and spreads out as a sheet of fluid flowing through the air. Spielbauer [1], in his Doctoral work at the Institute of Paper Science and Technology, conducted an experimental study of the mechanisms leading to the breakup of the black liquor sheet into droplets. He found that the initial step in the breakup process results from the growth of waves in the sheet of black liquor. As these waves grow, localized thin spots occur which spontaneously rupture (either due to air bubbles in the black liquor, small non-wettable particles in the black liquor, or some other undetermined cause). These perforations in the sheet then grow due to surface tension forces, intersect with neighboring holes, and form a network of strands. Finally, the strands become unstable and breakup into droplets [1].

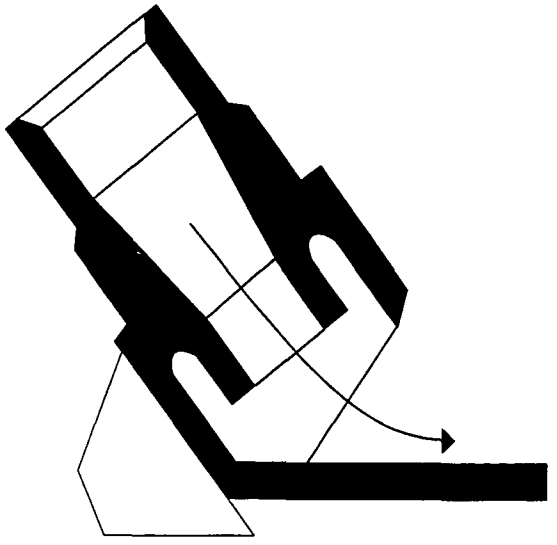

Figure 1. Schematic of a splash-plate black liquor spray nozzle.

We have developed a computational fluid dynamics approach which allows us to study the phenomenon of the growth of waves in the free surface. With the assumptions that the flow is isothermal and incompressible, we begin with the continuity equation,

$$\nabla \cdot \mathbf{v} = 0, \tag{1}$$

arising from conservation of mass and the Navier-Stokes equation (NSE),

$$\frac{\partial \mathbf{v}}{\partial t} + \mathbf{v} \cdot \nabla \mathbf{v} = \mathbf{g} - \frac{1}{\rho} \nabla P + \nu \nabla^2 \mathbf{v}, \tag{2}$$

derived from conservation of momentum, where $\mathbf{v}$ is the velocity vector, $\mathbf{g}$ is a body force vector, P is the pressure, ρ is the density, and ν is the kinematic viscosity. These equations are solved in the liquid phase, subject to boundary conditions at the edges of the computational domain, along interior obstacles, and at the interface between the liquid and vapor phases.

To completely describe the hydrodynamic instability leading to sheet breakup, it is also necessary to compute the velocity and pressure fields in the vapor phase. With the assumptions that the vapor phase is inviscid and the flow in the vapor phase is irrotational (which it must be if the vapor phase is initially stagnant), the vapor phase may be modeled using potential flow,

$$\nabla^2 \phi_v = 0, \tag{3}$$

where ϕ_v is the vapor phase potential. The pressure and velocities in the vapor phase are defined as

$$p_v = -\rho_v \frac{\partial \phi_v}{\partial t} \tag{4}$$

and

$$\mathbf{v}_v = \nabla \phi_v. \tag{5}$$

Therefore, in the vapor phase, we must solve Laplace's

equation, (3), with Neuman (derivative) boundary conditions in a region with curved boundaries. This is accomplished using standard second order accurate finite difference formulas for (3) in the bulk of the vapor phase and adjacent to straight boundaries. At the interface between the two fluids, a more complex treatment is required as we will describe below.

The interfacial boundary conditions are derived from stress and velocity balances. We begin the definition of the stress balances by defining an auxiliary height function, $H(x,y)$, for the location of the interface,

$$H(x,y) \equiv y - \eta(x) = 0. \tag{6}$$

The surface normal vector, $\mathbf{n} = (n_x, n_y)$, is computed from gradient of $H(x,y)$, which leads to the unit normal vector:

$$n_x = -\eta'\left(\eta'^2+1\right)^{-1/2},\ n_y = \left(\eta'^2+1\right)^{-1/2}, \tag{7}$$

where $\eta' = \partial\eta/\partial x$. The unit tangential, $\mathbf{t} = (t_x, t_y)$, vector is then computed from the orthogonality

$$t_x = \left(\eta'^2+1\right)^{-1/2},\ t_y = \eta'\left(\eta'^2+1\right)^{-1/2}. \tag{8}$$

Finally, the surface curvature, κ, may be computed from the divergence of the unit normal vector as

$$\kappa = \eta''\left(\eta'^2+1\right)^{-3/2}. \tag{9}$$

With these definitions in mind and the assumption of an inviscid vapor phase, the boundary conditions at the interface arising from normal and tangential stress balances are

$$P_\ell - \mathbf{n}\cdot\tau_\ell\cdot\mathbf{n} = P_v - \sigma k \tag{10}$$

and

$$\mathbf{t}\cdot\tau_\ell\cdot\mathbf{n} = 0, \tag{11}$$

respectively. The subscripts ℓ an v refer to the liquid and vapor phases, respectively, σ is the surface tension, and

$$\tau = 2\mu\left(\frac{\partial v_i}{\partial x_j} + \frac{\partial v_j}{\partial x_i}\right) \tag{12}$$

is the viscous stress tensor.

The remaining boundary condition at the interface is due to continuity of velocity. The normal velocity balance is given by

$$\mathbf{v}_\ell\cdot\mathbf{n} = \mathbf{v}_v\cdot\mathbf{n}. \tag{13}$$

Since the vapor phase is assumed to be inviscid, continuity of the tangential component of velocity cannot be imposed.

The remaining piece needed to completely define the problem is a method for tracking the interface between the liquid and vapor phases. Many methods are available and reviews can be found in [2] and [3]. In our work, we use the Volume of Fluid (VOF) technique [4] for tracking the location of the liquid phase as it is transported through a fixed Eulerian computational mesh. The VOF method has the advantage of simplicity in treating flows with large deformations and folding free surfaces. In order to increase the range of problems which can be accurately studied with this technique, we have extended the SOLA-VOF [5] method to include the viscous terms in the interfacial boundary condition and, with the assumptions about the vapor phase outlined above, allow flow of the vapor phase. As we will show below, the consideration of the vapor phase flow and variations in pressure are critically important for stability analysis.

The VOF method is derived from the first generally successful volume tracking free surface program, the Marker and Cell (MAC) method [6]. The MAC method tracks the location of the fluid within a fixed Eulerian mesh through the use of massless marker particles. These particles are convected through the computational domain at the end of each time step using the interpolated local fluid velocity. The free surface is then constructed from the cells partially filled with marker particles and having neighboring empty cells. In the MAC method, the normal stress boundary condition at the interface is simplified to

$$p_\ell = p_v. \tag{14}$$

This simplified boundary condition, applied at the cell center rather than the actual interface location, greatly reducing the accuracy of the computational technique.

The MAC method has evolved into the VOF technique which can be looked upon as the limit when the number of marker particles becomes infinite. Thus, the liquid is tracked by a step function, F, representing the fraction of each computational cell occupied by liquid. Transport of F through the computational mesh is governed by the F-convection equation,

$$\frac{\partial F}{\partial t} = -\mathbf{v}\cdot\nabla F, \tag{15}$$

which ensures that the amount of each phase is conserved.

The interface between the phases is determined on a cellwise basis from local F values. Cells with F=1 are liquid cells, cells with F=0 are vapor cells, and cells with intermediate values of F are free surface cells. Once the free surface cells have been identified, the location and shape of the interface within the free surface cells may be reconstructed from gradients of the F function.

The original VOF implementation, [5], included the effects of surface tension yielding Laplace's formula

$$P_\ell = P_v - \sigma\kappa \tag{16}$$

as the interfacial condition. In addition, this technique incorporated an interpolation scheme for applying the boundary condition at the free surface location rather than the center of the computational cell. Improvements in algorithms for computing surface curvature and methods for treating obstacles within the computational domain were incorporated in a subsequent program [7] followed by extension to three dimensions for cylindrical coordinates [8]. All three of these programs neglect the viscous component of the liquid normal

stress in the liquid phase at the interface and assume that the pressure in the vapor phase remains constant. These assumptions limit application of these programs to problems where the viscous component of the interfacial condition is unimportant and where the pressure variations in the vapor phase can safely be neglected.

In the study of free surface flows such as the die-swell problem [9], inclusion of the viscous terms in the interfacial boundary condition is vital [10, 11]. Therefore, implementations which neglect these components are unable to accurately solve the die-swell problem. In addition, in the study of the stability of thin liquid films, the viscous terms at the interface and variations in the vapor phase pressure along the interface are the primary factors inducing instability and wave growth [12].

For these reasons, we have extended the VOF technique to allow inclusion of the viscous terms in the liquid phase at the interface and to allow variation of the pressure in the vapor phase. We will outline the various solution algorithms used and the implementation of the viscous component of the interfacial condition. The numerical solution of the vapor phase flow coupled with the liquid phase will be presented with an examination of the combined technique's accuracy.

To test the ability of our method to treat problems involving the stability of two-phase shear flows, we study the stability of a thin liquid sheet flowing through an, initially stagnant, inviscid vapor phase. We accurately compute the growth rate of waves in a thin liquid sheet in agreement with predictions from linear stability analysis. This test problem demonstrates that, despite popular perception, the VOF method can be very accurate and reliable, when the complete interfacial conditions are considered.

NUMERICAL TECHNIQUE

We begin the description of the numerical technique with a brief outline of the solution algorithm employed in the SOLA family of programs. This is followed by a description of the additions we have made to improve the accuracy and extend the capabilities of our program, IPST-VOF3D: specifically, more accurate methods for differencing the convective terms in the NSE, inclusion of the viscous terms in the liquid at the interface, and solution of the potential flow equations in the vapor phase to yield the pressure in the vapor phase.

In the SOLA family of programs, the velocity and pressure fields are solved on a staggered grid (Figure 2). In this representation, vector quantities are stored on cell faces, and scalar quantities at the cell centers.

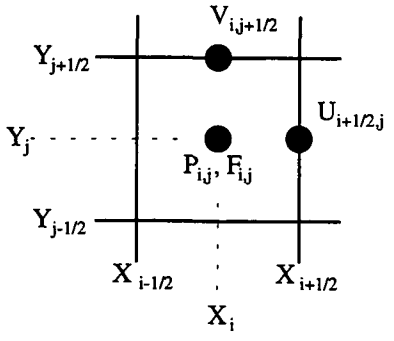

Figure 2. Schematic of computational grid geometry.

Here, we briefly describe the numerical method, consisting of a two step projection, used to solve the NSE in the SOLA family of programs. Generally, this can be described by defining an explicit guess,

$$\tilde{\mathbf{v}}^n = \mathbf{v}^n + \delta t\left[\mathbf{g} - \frac{1}{\rho}\nabla P^n + \nu\nabla^2\mathbf{v}^n - \mathbf{v}^n\cdot\nabla\mathbf{v}^n\right], \qquad (17)$$

for the new velocity field, where the superscript refers to the time step. Except as described below for the convective terms, the specifics of the finite difference representations used can be found in Refs. [5], [7], and [8]. The velocity field after the time step can then be written as the explicit guess plus a correction due to the pressure change across the time step,

$$\mathbf{v}^{n+1} = \tilde{\mathbf{v}}^n - \frac{\delta t}{\rho}\nabla\left(\delta P^{n+1}\right). \qquad (18)$$

Since mass must be conserved at all times, we may substitute (18) into (1) yielding

$$\frac{\delta t}{\rho} V\nabla\cdot\left[\nabla\left(\delta P^{n+1}\right)\right] = V\nabla\cdot\tilde{\mathbf{v}}^n, \qquad (19)$$

where V is the volume of the computational cell, needed to ensure a symmetric system of equations [7]. The Poisson equation for pressure, (19), yields a sparse, symmetric linear system which can be solved using a variety of numerical methods such as successive over-relaxation (SOR) or the Conjugate Residual (CR) method [8]. With the new pressure field available, the corrected velocity field is then computed from (18).

The F-convection equation, (15), is solved using donor-acceptor differencing [8] to assist in maintaining a sharp interface between the liquid and the vapor phases. Once the new fluid configuration has been obtained, it is possible to reconstruct the localized interface configuration needed for computation of surface tension force [8]. Again, the details of this process are presented elsewhere [5, 7, and 8].

As we have shown previously [9], as the Reynolds number increases, the accuracy of the finite difference representation of the convective terms in the NSE limits the accuracy of the entire solution. Therefore, in addition to the standard

differencing for the convective terms present in the SOLA programs, we applied and evaluated three third order accurate differencing options Quadratic Upstream Interpolation for Convective Kinematics (QUICK) [13, 14], third order accurate upwind differencing (THIRD) [3, 15], and the method of Kawamura and Kuwahara (KANDK) [3, 16]. The details of these differencing techniques are presented elsewhere [3, 9].

The previous VOF techniques used Laplace's formula, (16), as a simplified formula for the normal stress balance. To eliminate the assumption inherent in (16) that the viscous terms in the interfacial boundary condition are negligible, we have included an option for computing the viscous forces. The local unit vector normal to the interface is computed in the manner described above. Once the coordinate axis most nearly normal to the interface has been determined, a local height function analogous to (6) is computed and the unit surface normal is obtained from (7).

Next, the components of the viscous stress tensor, (12), are computed using the provisional velocities, $\tilde{\mathbf{v}}_\ell^n$, where only velocities within the liquid phase are included in the finite difference formulas. Finally, the viscous component of the interfacial boundary condition is computed from $\mathbf{n}\cdot\boldsymbol{\tau}_\ell\cdot\mathbf{n}$.

POTENTIAL FLOW IN THE VAPOR PHASE

As stated above, for stability problems such as flow of a thin liquid sheet, allowing the pressure in the vapor phase to vary is vital. We have implemented a method for solving the potential flow equation in the vapor phase which is coupled to the full NSE in the liquid phase through the interfacial conditions. This allows computation of the pressure in the vapor phase as a function of time and position.

The major challenge in solving the vapor phase potential equation, (3), is the imposition of the Neuman boundary conditions along the curved boundary made up of the interface between the liquid and vapor phases. We have implemented a modified form of Bramble and Hubbard's [17] second order accurate method for solving Poisson's equation in a region with curved boundaries having mixed boundary conditions. Bramble and Hubbard [17] define a second order accurate operator,

$$\delta_n\phi_0 = \phi_0\sum_{i=1}^{3}a_i - \sum_{i=1}^{3}a_i\phi_i\,, \tag{20}$$

for the normal derivative using three points within the region of interest (in this case the vapor phase). The coefficients, a_i, are determined from solution of the system of equations:

$$\begin{bmatrix} \bar{y}_1 & \bar{y}_2 & \bar{y}_3 \\ \bar{x}_1 & \bar{x}_2 & \bar{x}_3 \\ \bar{x}_1^2-\bar{y}_1^2 & \bar{x}_2^2-\bar{y}_2^2 & \bar{x}_3^2-\bar{y}_3^2 \end{bmatrix}\begin{bmatrix} a_1 \\ a_2 \\ a_3 \end{bmatrix} = \begin{bmatrix} 1 \\ 0 \\ 0 \end{bmatrix}, \tag{21}$$

where $\bar{y}$ and $\bar{x}$ are the distances from the surface point to neighboring points within the flow in the normal and tangential directions, respectively. In addition, Bramble and Hubbard [17] present criteria which, when satisfied, ensure that the operator yields a diagonally dominant system of equations.

The boundary condition for the vapor phase potential at the interface is conservation of the normal velocity, (13). Thus, the boundary operator is equal to the normal velocity in the liquid phase plus a small correction arising from the derivation

$$\delta_n\phi_0 = v_{\bar{y}} + \frac{\partial v_{\bar{y}}}{\partial \bar{x}}\sum_{i=1}^{3}a_i\bar{x}_i\bar{y}_i\,, \tag{22}$$

where $v_{\bar{y}}$ is the normal velocity at the interface and $\partial v_{\bar{y}}/\partial\bar{x}$ is the tangential derivative of the normal velocity at the interface [17]. Again, since we have assumed that the vapor phase is inviscid, no restrictions are placed on the tangential velocity in the vapor phase at the interface.

With incorporation of the liquid phase viscous terms and variations in the vapor phase pressure in the interfacial boundary condition, the solution procedure becomes:

1. Compute the surface curvature from the local liquid configuration.
2. Compute the surface normal velocity from the change in surface position.
3. Solve (3) for the vapor phase potential.
4. Compute the vapor phase pressure from (4).
5. Compute the explicit guess for the liquid phase velocity field from (17).
6. Compute the interfacial liquid phase stress from (12).
7. Compute the pressure on the liquid side of the interface from (16).
8. Solve the Poisson pressure equation, (19), yielding the liquid phase pressure field.
9. Update the liquid phase velocity field using (18).
10. Solve (15) to yield the new fluid configuration.

These steps may be repeated until the desired time is reached. The second and third steps have been added to allow for variations in the vapor phase pressure and the fifth step is required for inclusion of the liquid phase viscous terms in the interfacial conditions.

RESULTS AND DISCUSSION

To test the implementation of the coupled inviscid vapor phase with the full NSE in the liquid phase, we study the stability of thin liquid sheet flowing through an inviscid vapor phase as presented in Figure 3.

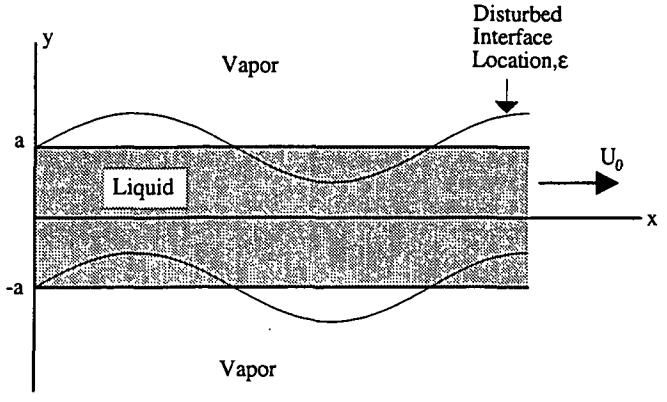

Figure 3. Schematic of sheet instability problem.

The variation in the surface position, ε, shown in Figure 3 is assumed to be of the form

$$\varepsilon = \varepsilon_0 e^{\omega t + ikx} \tag{23}$$

where ε_0 is the initial amplitude, $\omega = \omega_r + i\omega_i$ is the complex growth rate, $i = \sqrt{-1}$, and k is the wavenumber of the disturbance. Study using linear stability analysis [12] yields dispersion relations between the wavenumber and the growth rate for antisymmetric,

$$0 = \left(\tilde{\omega}_1 + 4\omega^2 Z\right)\tilde{\omega}_1 \tanh(m) + \tilde{\rho}\tilde{\omega}^2 + m^3 + 4m^3 Z^2\left[m\tanh(m) + \sqrt{m^2 + \tilde{\omega}_1/Z}\tanh\sqrt{m^2 + \tilde{\omega}_1/Z}\right] \tag{24}$$

and axisymmetric,

$$0 = \left(\tilde{\omega}_1 + 4\omega^2 Z\right)\tilde{\omega}_1 \coth(m) + \tilde{\rho}\tilde{\omega}^2 + m^3 + 4m^3 Z^2\left[m\coth(m) + \sqrt{m^2 + \tilde{\omega}_1/Z}\coth\sqrt{m^2 + \tilde{\omega}_1/Z}\right] \tag{25}$$

disturbances. Where $\tilde{\omega} = \tilde{\omega}_r + i\,We_\ell^{1/2}\tilde{\omega}_i$, $\tilde{\omega}_1 = \tilde{\omega} + i\,We_\ell^{1/2} m$, $\tilde{\omega}_r = \omega_r\left(\rho_\ell a^3/\sigma\right)^{1/2}$, $\tilde{\omega}_i = \omega_i\left(a/U_0\right)$, a is the initial sheet half-thickness, $m = ka$ is the dimensionless wavenumber, and U_0 is the initial sheet velocity. The remaining parameters are defined as the Weber number, $We_\ell = \rho_\ell U_0^2 a/\sigma$, the Ohnesorge number, $Z = \mu_\ell\left(\rho_\ell a\sigma\right)^{-1/2}$, and the density ratio, $\tilde{\rho} = \rho_g/\rho_\ell$.

It is possible to numerically solve the dispersion relations for given We_ℓ, Z, and $\tilde{\rho}$ to yield the complex growth rate, $\tilde{\omega}$, as a function of the dimensionless wave number, m. The real part of $\tilde{\omega}$ is dimensionless growth rate of a disturbance with wavenumber m. Results for We_ℓ=40, Z=0.1, and $\tilde{\rho}$ =0.1 are shown in Figure 4 for both antisymmetric and axisymmetric disturbances represented by solid and dashed lines, respectively. The data points plotted on Figure 4 represent our computed results, with the filled circles resulting from antisymmetric disturbances and the open circles from axisymmetric disturbances.

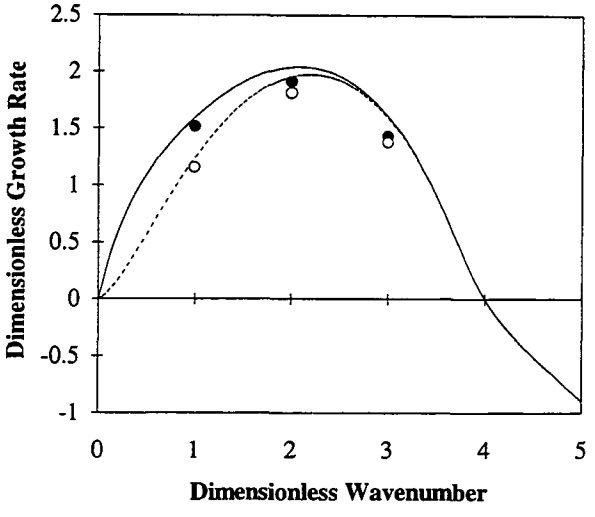

Figure 4. Non-dimensional growth rate for We_ℓ=40, Z=0.1, and $\tilde{\rho}$ =0.1 obtained from numerical solution of Li and Tankin's [12] dispersion relations. Open and closed circles represent results of our computational analysis.

CONCLUSIONS

The instability leading to breakup of a sheet of black liquor is an important step in the droplet formation process. We have developed a computational technique based on solution of the full Navier-Stokes equations in the liquid phase coupled with a potential flow solution in the vapor phase. This technique can be used to study the physical processes leading to this instability.

REFERENCES

1. Spielbauer, T. M., *The Stability and Disintegration of Radially Thinning Liquid Sheets*, Doctoral Dissertation, Institute of Paper Science and Technology, Atlanta, 1992.

2. Floryan, J. M. and Rasmussen, H., "Numerical Methods for Viscous Flows with Moving Boundaries," *Applied Mechanics Reviews*, 42: 323(1989).

3. McKibben, J. F., *A Computational Fluid Dynamics Model for Transient Three-Dimensional Free Surface Flows*, Doctoral Dissertation in progress, Institute of Paper Science and Technology, Atlanta, 1993.

4. Hirt, C. W. and Nichols, B. D., "Volume of Fluid (VOF) Method for the Dynamics of Free Boundaries," *Journal of Computational Physics*, 39: 201(1981).

5. Nichols, B. D., Hirt, C. W., and Hotchkiss, R. S., *SOLA-VOF: A Solution Algorithm for Transient Fluid Flow with Multiple Free Boundary*, Los Alamos Report LA-8355, Los Alamos National Laboratory, 1980.

6. Harlow, F. H. and Welch, J. E., "Numerical Calculation of Time-Dependent Viscous Incompressible Flow of Fluid with Free Surface," *Physics of Fluids*, 8: 2182(1965).

7. Torrey, M. D., Cloutman, L. D., Mjolsness, R. C., and Hirt, C. W., *NASA-VOF2D: A Computer Program for Incompressible Flows with Free Surfaces*, Los Alamos Report LA-10612-MS, Los Alamos National Laboratory, 1985.

8. Torrey, M. D., Mjolsness, R. C., and Stein, L. R., *NASA-VOF3D: A Three-Dimensional Computer Program for Incompressible Flows with Free Surfaces*, Los Alamos Report LA-11009-MS, Los Alamos National Laboratory, 1987.

9. McKibben, J. F. and Aidun, C. K., "Computational Visualization of Three-Dimensional Free-Surface Flows," *Proceedings 1991 TAPPI Engineering Conference*, TAPPI Press, Atlanta, 1991.

10. Hill, G. A., *Numerical Simulation of Free Surface Flows*, Doctoral Dissertation, University of Saskatchewan, Saskatoon, 1979.

11. Hill, G. A., Shook, C. A., and Esmail, M. N., "Finite Difference Simulation of Die Swell for a Newtonian Fluid," *Canadian Journal of Chemical Engineering*, 59: 100(1981).

12. Li, X. and Tankin, R. S., "On the Temporal Instability of a Two-Dimensional Viscous Liquid Sheet," *Journal of Fluid Mechanics*, 226: 425(1991).

13. Leonard, B. P., "A Stable and Accurate Convective Modeling Procedure Based on Quadratic Upstream Interpolation," *Computer Methods in Applied Mechanics and Engineering*, 19: 59(1979).

14. Freitas, C. J., Street, R. L., Findikakis, A. N., and Koseff, J. R., "Numerical Simulation of Three-Dimensional Flow in a Cavity," *International Journal for Numerical Methods in Fluids*, 5: 561(1985).

15. Agarwal, R. K., "A Third-Order-Accurate Upwind Scheme for Navier-Stokes Solutions at High Reynolds Numbers," *AIAA Paper AIAA-81-0112*, 1981.

16. Kawamura, T. and Kuwahara, K., "Computation of High Reynolds Number Flow Around a Circular Cylinder with Surface Roughness," *AIAA Paper AIAA-84-0340*, 1984.

17. Bramble, J. H. and Hubbard, B. E., "Approximation of Solutions of Mixed Boundary Value Problems for Poisson's Equation by Finite Differences," *Journal of the Association of Computing Machinery*, 12: 114(1965).

ACKNOWLEDGMENTS

This study is supported by industrial contributions and the National Science Foundation under grant CTS-9258667. The computations were conducted, in part, using the Cornell National Supercomputer Center, a resource of the Center for Theory and Simulation in Science and Engineering at Cornell University, which is funded in part by the National Science Foundation, New York State, and the IBM Corporation. Portions of this work were used by J.F.M. as partial fulfillment of the requirements for the Ph.D. degree at the Institute of Paper Science and Technology.